Applied Catalysis B: Environmental 187 (2016) 350–356

Contents lists available at ScienceDirect

Applied Catalysis B: Environmental

journal homepage: www.elsevier.com/locate/apcatb

Photodegradation mode of stearic acid crystal on heterogeneous anatase/amorphous titania films observed by differential interference contrast microscopy

Fouad Araiedh[a,b], Franck Ducos[b], Ammar Houas[a,c], Nouari Chaoui[b,*]

[a] Unité de Recherche Catalyse et Matériaux pour l'Environnement et les Procédés (URCMEP), Université de Gabès, Campus Universitaire—Cité Erriadh, 6072 Gabès, Tunisia
[b] Laboratoire de Chimie et Physique-Approche Multi-échelle des Milieux Complexes (LCP-A2MC) Université de Lorraine, France
[c] Al Imam Mohammad Ibn Saud Islamic University (IMSIU), College of Sciences, Department of Chemistry, Riyadh 11623, Saudi Arabia

ARTICLE INFO

Article history:
Received 12 October 2015
Received in revised form 11 January 2016
Accepted 16 January 2016
Available online 25 January 2016

Keywords:
Photocatalysis
Optical microscopy
TiO_2 thin film
Stearic acid

ABSTRACT

Reflected-light differential interference contrast microscopy was used to observe the disappearance of stearic acid crystal (B-polymorph) deposited onto a heterogeneous anatase/amorphous titania film upon ultraviolet light exposure. Microstructural studies of the films demonstrate the formation of anatase microdomains with sub-micrometric size randomly distributed throughout the amorphous surface of the film. The microscopy images reveal that the disappearance of stearic acid crystal is initiated in the immediate vicinity of these microdomains located within the crystal or close to its edges. The stearic acid disappearance proceeds via lateral growth and coalescence of pits in shape of flattened-hexagons showing a preferential orientation with respect to the stearic acid crystal symmetry. This latter fact, which is observed for the first time to the best of our knowledge, is explained by the dependence on crystallographic orientation of the progression rate of the pit edges. To justify the observed photodegradation mode, we first invoke the ultraviolet-induced formation of radical species at the anatase microdomains and their diffusion towards the pits edges. Then, the geometry and the preferential orientation of the pits are discussed in terms of anisotropy of intermolecular interactions within the crystal. These results suggest that the energy barrier seen by the radical species reaching the pit edges is correlated to the crystallographic orientation with consequences on the reaction kinetics.

1. Introduction

Titanium dioxide is well-known as a material of choice for self-cleaning surfaces because of its favorable physical and chemical properties. As a thin layer, the photocatalytic performances of titania are often estimated by measuring the evolution of the concentration of organic contaminants initially deposited onto its surface as a function of ultraviolet irradiation time [1–4]. Since the pioneer work of Paz and Heller [1], one the most popular contaminants used is stearic acid ($CH_3(CH_2)_{16}COOH$) because of its stability under ultraviolet irradiation and its low vapor pressure. Several studies have established that the degradation mode of stearic acid (SA, hereafter) on titania thin films is strongly influenced by the structure and morphology of the surface at various scales [5–7] but also the morphology of the SA deposits [6,8]. Sawunyama et al. [6] compared the decomposition of a partial and full monolayer of SA on titania using in situ atomic force microscopy (AFM, hereafter). Their measurements revealed an inhomogeneous reactivity pattern at the nanometer scale attributed to randomly distributed active centers. In a previous work [8]. we pioneered the use of standard optical microscopy to observe the photocatalyzed degradation of SA islands deposited on a continuous anatase coating at the micrometric scale. We observed that the photodecomposition of individual islands proceeded from the edges towards the center according to a zero-order kinetics with respect to island area. These studies have shown that the direct observation at various scales of the degradation mode of SA deposited on titania can provide new insights in the study of the factors that control the kinetics and mechanisms of photocatalysis.

This has motivated a great part of this work which considers an original and interesting SA/photocatalyst configuration. We prepared by sol gel route heterogeneous anatase/amorphous titania films according to a protocol reported by Bahtat et al. [9]. The as-prepared film consists of a non-photoactive amorphous tita-

* Corresponding author.
E-mail address: nouari.chaoui@univ-lorraine.fr (N. Chaoui).

http://dx.doi.org/10.1016/j.apcatb.2016.01.039
0926-3373/

nia matrix with randomly distributed anatase microdomains with sub-micrometric size. We use reflected-light differential interference contrast (RL-DIC) to visualize the ultraviolet photocatalytic degradation mode of well-crystallized stearic acid (B polymorphs) initially grown on the film surface. The RL-DIC microscopy is capable of producing high-contrast images (high-edge definition) of transparent medium and is therefore useful for the observation of stearic acid on titania surface. Furthermore, this technique allows the microscope to achieve high-resolution images at large aperture sizes enabling, at the same time, the observation of the anatase microdomains (sub-micrometric scale). We show that the direct observation of the TiO_2 photocatalytic surface reaction, using RL-DIC microscopy, provides new insights into the reaction kinetics and degradation mechanisms of SA on TiO_2. Our results reveal that the photocatalyzed degradation of the SA crystals is initiated at anatase microdomains, proceeds along specific crystallographic directions and is mediated via the diffusion of active species.

2. Experimental

2.1. Preparation of the TiO_2 thin films

2.1.1. Preparation of TiO_2 sol

Titanium tetra-isopropoxide [$Ti(iOC_3H_7)_4$] (Aldrich, 97%) was used as a precursor to synthesize the titania sol via an acid catalyzed sol-gel process. The TiO_2 sol was prepared according to a procedure reported by Bahtat et al. [9]. Briefly, 4.65 ml of propan-2-ol (Aldrich, 99.8%) was added drop by drop, under magnetic stirring, in 1.6 ml of TTiP. The solution was left under closed agitation under heating at 60 °C. After 15 min, 5.15 ml of acetic acid (ACROS Organics, 99.5%) was added for 10 min under heating at 60 °C. Finally, 12 ml of methanol (VWR, 100%) was poured and the solution was further stirred for 2 h. The sol was aged during 24 h. The obtained TiO_2 sol was transparent, stable and very fluid for several weeks. Its resulting pH was in the range 2–3.

2.1.2. Dip coating

Prior to coating, the glass substrates were cleaned in ultrasonic bath with detergent and successively rinsed with distilled water and absolute ethanol grade. The sol was dip coated onto borosilicate glass substrates (64 mm × 22 mm × 0.5 mm). The sol was deposited at a withdrawal speed of 100 mm/min. and the procedure was repeated eight times in order to obtain a film thickness of about 120–150 nm. Then, the film was then dried at 100 °C during one hour and was finally calcined at 450 °C for two hours.

2.2. Characterization of the films

The crystal structure and crystallinity of the TiO_2 catalysts were determined by micro-raman spectrometry (Jobin Yvon Horiba, LabRAM HR evolution). The excitation laser wavelength was 633 nm. The power used was voluntarily kept at the minimum in order to be well below the power level needed to induce crystallization. The topography of TiO_2 thin films was investigated by atomic force microscopy (AFM, Pacific Nanotechnology) with a silicon nitride tip in tapping mode.

2.3. Photocatalytic experiment

2.3.1. Stearic acid deposition

Stearic acid film was dip-coated onto the titania photocatalyst from a 0.06 M stearic acid methanolic solution. The sample was dipped twice at a withdrawal speed of 100 mm/min in the solution at 30 °C and dried for two hours in ambient atmosphere.

2.3.2. Photocatalytic degradation

The photodegradation of the SA layer was performed using the ultraviolet light from a 200 W mercury-xenon lamp simulating solar radiation equipped with a 0.5 m length optical fiber. The power density in the UVA was 2.5 mW/cm^2, as measured by a photo-radiometer (Delta Ohm DO 9021) equipped with UVA head.

2.3.3. Reflected light-differential interference contrast (RL-DIC) microscopy

The samples were observed with a reflected-light differential interference contrast microscope (Axio Imager A1m from Zeiss) equipped with a high-resolution camera (AxioCam MRc5). The principle of this technique is based on the interference of very closely-spaced and linearly cross-polarized beams that transform thickness *gradient* or refractive index *gradient* or both in an image with shadow-cast appearance. This effect enables a contrast enhancement of edges and the observation of minute features in transparent objects (SA crystal here) with high contrast and high resolution.

3. Results

3.1. Characterization of the titania film

Fig. 1(a) shows a RL-DIC microscopy image of the sol-gel titania film dip-coated (eight layers) on borosilicate glass and heat treated at 450 °C for 2 h. The surface of the film shows a constellation of dark spots surrounded by white halos on a homogenous background and uniformly distributed on the film surface. Their diameter varies from a few hundreds nanometer to one micrometer. Except for these black spots, the rest of surface appears featureless at this scale.

A representative AFM image of the surface of the TiO_2 film is shown in Fig. 1(b). The AFM images reveal a surface with clearly visible microdomains with size ranging from 300 nm up to one micrometer emerging from the surface of the film. The heights of these microdomains with respect to the surface of the film typically vary from a few tens to a hundred of nm as shown by the image profiles. A close inspection of the flat regions also reveals minute hollows structures (surrounded in white) with diameters ranging from tens to a few hundreds of nanometres and approximately ten nm deep as shown by the image profile. It is striking how the forms of the microdomains and the hollows, whatever their sizes, are alike strongly suggesting a common origin. One can also appreciate a preferential orientation of both microdomains and hollows. Fig. 1(c) presents representative micro-raman spectra of a microdomain and a flat region of the titania film. The spot size of the laser on the film surface was about 1 μm in diameter. The power of the laser used was voluntarily kept at the minimum in order to be well below the power level needed to induce crystallization. This explains the overall low signal/noise ratio in the recorded spectra. The Raman spectra of the microdomains show a sharp and strong line at 142 cm^{-1} and four other much weaker lines at 196, 398, 515 and 638 cm^{-1} which are characteristic of the anatase phase [10]. The Raman signal of the flat region at least 10 μm away from any visible microdomain is considerably reduced compared with that of the microdomains so that only a weak line at 196 cm^{-1} is observed. This strongly suggests that the degree of crystallinity of the flat region is much weaker and supports the fact that the observed hollows may be attributed to fine anatase grains embedded in an amorphous matrix.

In our study, the films were prepared in accordance with the procedure proposed by Bahtat et al. [9] except for the duration of the thermal treatment at 450 °C which was 2 h in our work instead of 15 min. These authors observed spherical nanocrystals of about

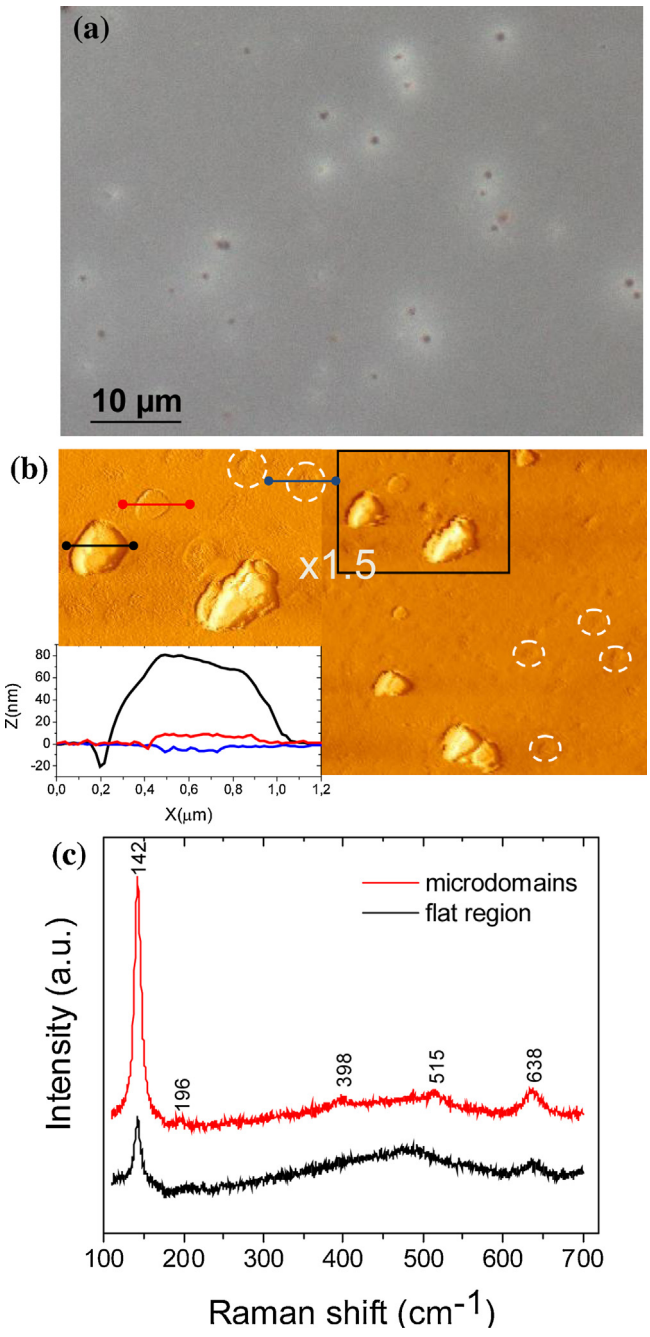

Fig. 1. (a) RL-DIC microscopy image of the sol-gel titania film dip coated on borosilicate glass and heat-treated at 450 °C for 2 h in air. (b) AFM image of film surface and representative profiles of the microdomains and hollows (c) Representative micro-Raman spectra of the microdomains and the flat region of the film.

5 nm in diameter embedded in an amorphous matrix. The observation of microdomains with diameter ranging from a few hundreds of nanometres up to one micrometre in Fig. 1(b) is consistent with the work of Exarhos and Aloi [11] who studied the isothermal crystallization of sol-gel deposited amorphous titania film. According to these authors, the crystallization occurs at nucleation centres which either pre-exist in the amorphous phase or are formed during the treatment. After several hours of isothermal annealing at 350 °C, the microstructure of their film showed a distribution of round spherical anatase particles with 100–200 nm diameters embedded in a fine-grained amorphous matrix and surrounded by a thin void shell. This strongly suggests that the observed hollows are related to the crystallisation of embedded particles that can further growth and/or coalesce to form larger the observed microdomains.

3.2. Photocatalytic activities

3.2.1. RL-DIC microscopy observation of SA crystals prior to ultraviolet exposure

Fig. 2(a) presents RL-DIC microscopy images of a SA crystal grown on the titania film prior to ultraviolet exposure. As shown by the central panel of Fig. 2(a), the SA crystal is flat, rhombus-shaped and presents an obtuse angle of 107° (and thus an acute angle of 73°). The identification of SA polymorphs can be easily performed, carried out by observing the crystal shape [12–15]. Both B and C polymorphs form plate rhombus-shaped crystals which can be clearly distinguished from their acute angle which is about 74° for the B and close to 54° for the C polymorph. Therefore, the measured angle is consistent with the B-polymorph of SA.

The colour contrast between the crystal (pale brown) and the background (light blue) observed in Fig. 2(a) is a manifestation of the strong interaction between the polarized light and the SA crystal [16] that is birefringent. Due to the thickness of the crystal and its orientation in the plan of the microscope stage, phase difference is generated between the ordinary and extraordinary beams, inherent to its birefringence, explaining the observed colour contrast. The colour variation on the RL-DIC micrograph can be then correlated with the thickness of the crystal. As a result, the regions of the crystal showing homogenous pale brown colour present a constant thickness.

The magnitude of the image (×1000) enables the resolution of submicrometric features and makes possible the observation of the previously described microdomains which appear as minute dark points surrounded by a white halo on the image background. It is also worth noting that several microdomains are very close to crystal edge as indicated by the black arrows on the left panel of Fig. 2(a). Their distance to the crystal edge is of the order of 1 µm. On the other hand, a close inspection of the picture reveals anatase microdomains distributed within the crystal as seen by the magnification of the image in the right panel of Fig. 2(a). Some of them are surrounded by a blue halo suggesting the existence of a gap between the microdomain and the crystal. An AFM image of a representative anatase microdomain within a SA crystal shown in Fig. 2(b) confirms this assumption. As expected, the blue halo is related to the presence of a dip in which the microdomain is almost centered. The dip presents a flattened-hexagon shape and is about 1 µm wide and 3 µm long. The profile of the dip allows an estimation of the thickness of the SA crystal which is about 30–40 nm thick. A possible explanation for the formation of such a dip is that the prevention of crystal growth due to the microdomains.

3.2.2. RL-DIC microscopy observation of SA crystals upon ultraviolet irradiation

Fig. 3 presents RL-DIC microscopy images of a SA crystal grown on the titania film upon ultraviolet irradiation. It is observed the pits widen as the exposure time is increased (Fig. 3(a)–(d)) strongly suggesting a photocatalyzed degradation of the SA crystal. This assumption is supported by the fact that the disappearance of SA is systematically initiated in the immediate vicinity of an anatase microdomain as shown by the magnifications in Fig. 3(a)–(d). It should also be noted that the dips present a more or less regular flattened-hexagon shape and show a preferential orientation towards the rhombus big axis. As the irradiation time is further increased, the lateral growth of the pits leads to coalescence (Fig. 3(e)) which results in percolation of the hexagons (Fig. 3(f)) and finally, the total disappearance of the SA crystal (Fig. 3(g)) as shown by the remaining background colour.

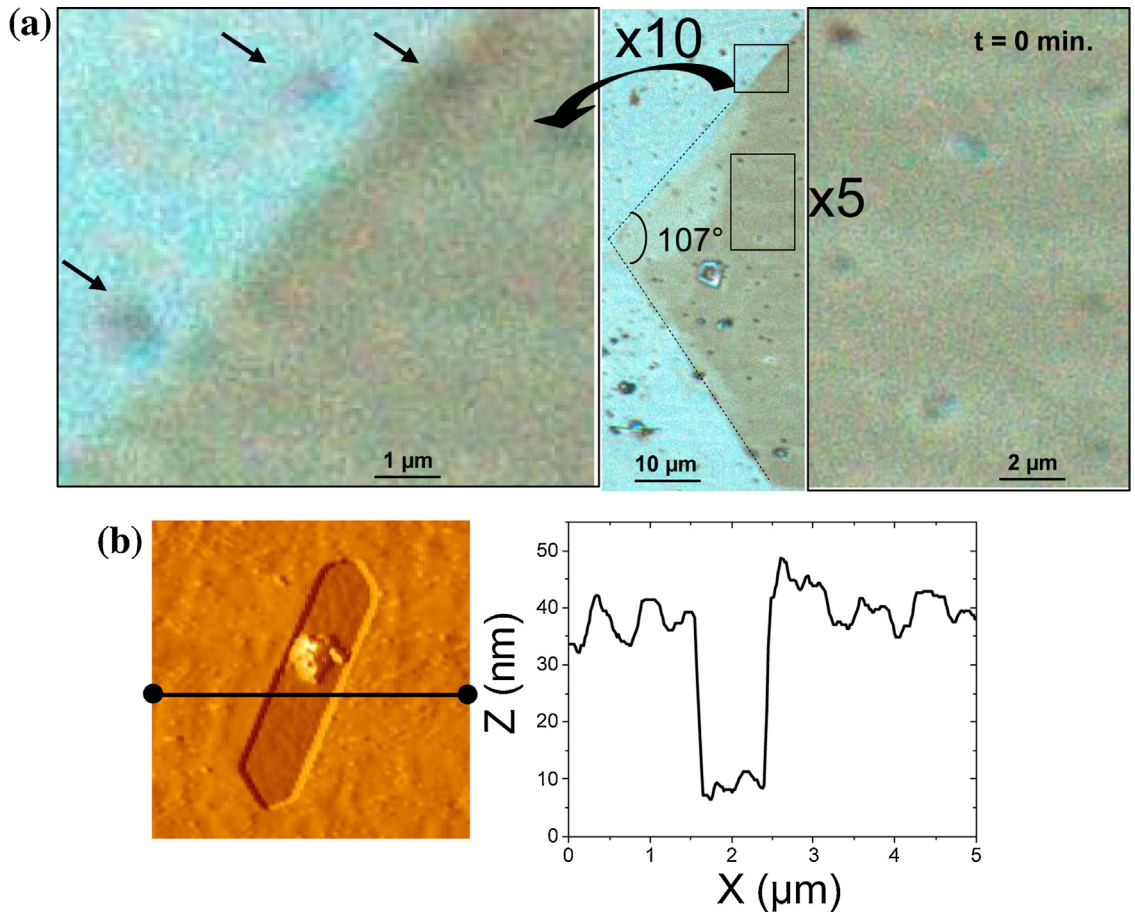

Fig. 2. (a) RL-DIC microscopy image of stearic acid crystal (B-polymorph) deposited on the titania film before ultraviolet irradiation. The left panel is a magnification (×10) of the edges of the crystal showing a microdomain at the edge and two others in its immediate vicinity. The left panel is a magnification (×5) of a region the crystal showing microdomains within the crystal. (b) AFM image of a microdomain at the centre of a dip within the crystal and profile of the dip.

Table 1
Crystallographic data for the B-polymorphs of stearic acid (from Ref. [15]).

Polytype	Structure	Space group	a (Å)	b (Å)	c (Å)	β (deg)
B_m	monoclinic	$P2_1/c$ Z = 4	43.95	7.397	5.598	90.31
B_o	orthorhombic	Pbca Z = 8	7.408	5.587	87.69	90

From the flattened hexagon orientation and the crystal symmetry, it is possible to determine the crystallographic orientation of the edges of the growing pits. Table 1 presents the crystallographic data of the B-polymorphs. The B-polymorph of SA presents two polytypes: one is monoclic (B_m) crystalizes in the $P2_1/c$ space group while the other one is orthorhombic (B_o) and crystalizes in the Pbca space group.

Fig. 4 presents the relationship between the crystal structure, the geometry and the orientation of the pits. For simplicity, we have only considered the case of the monoclinic B-polymorphs but the following descriptions can be easily transposed to the orthorhombic form of the B-polymorphs. Fig. 4(a) shows a RL-DIC microscopy image of a dip on which are indicated the characteristic angles of the B-polymorph. Fig. 4(b) shows the respective orientations and morphologies of the SA crystal and pit with respect to the unit-cell while Fig. 4(c) presents the projection of the unit-cell basal plane (bc plane) of the monoclinic B form adapted from Refs. [13,15]. The basal plane of the crystal corresponds to the {1 0 0} faces. The geometrical characteristic of the pits (flattened hexagons) is also consistent with the B-form. The four edges of the pit that are parallel to the four sides of the rhombus coincide with the {h11} faces and the two others correspond to the {h10} faces. The angle between $(0\,1\,1)$ and $[01\bar{1}]$ crystallographic directions as measured in the $(1\,0\,0)$ basal plane is 73° and that between $(0\,1\,1)$ and $[0\bar{1}1]$ is 107° in good agreement with the characteristic angles of the B-polymorph.

The gap distances $g_{\{h11\}}$ and $g_{\{h10\}}$ between the active domain and the pits edges according to {h11} and {h10} faces respectively, have been plotted as a function of irradiation time in Fig. 5. From 5 to 40 min., $g_{\{h10\}}$ and $g_{\{h11\}}$ increase linearly with irradiation time to reach 2.8 µm and 4 µm at 40 min, respectively. The displacement rates of the edges $R_{\{h11\}}$ and $R_{\{h10\}}$ according to the normal directions to the {h11} and {h10} faces, were found to be 0.069 and 0.057 µm min^{-1}, respectively. The fact that the intercepts of both regression lines have a positive value is consistent with the preexistence of the pits prior to the UV–vis irradiation (Fig. 2).

4. Discussion

The presented results provide further evidence that molecules well separated from a photoactive titania domain can be photodegraded. As earlier reported [17–19]. this remote photodegradation is mainly due to the surface diffusion of active species like hydroxide radicals ($OH^\bullet$) or even peroxide (H_2O_2) from the titania microdomain. These active species can diffuse at relatively large

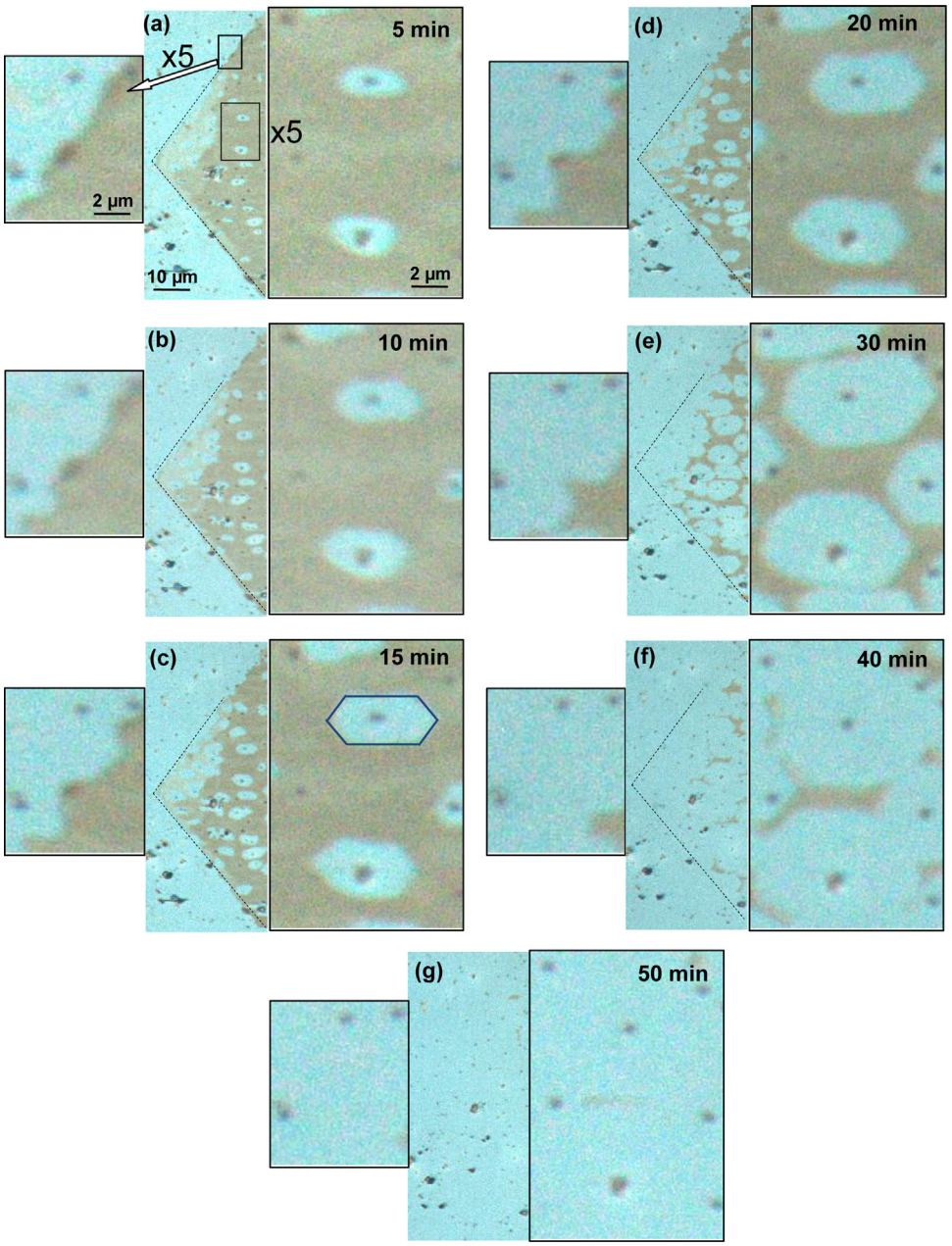

Fig. 3. RL-DIC microscopy image of stearic acid crystal (B-polymorph) deposited on the titania film upon ultraviolet irradiation after (a) 5 min, (b) 10 min, (c) 15 min, (d) 20 min, (e) 30 min, (f) 40 min and (g) 50 min exposure time.

distance, up to several tens μm and react with anchored molecules [17–19]. Unlike the above cited works, where the active domains present a linear edge with indefinite length making the species to diffuse towards the normal direction, the active microdomains described in our work are very limited (a few hundred nm) so that they could almost be considered as point diffusion sources. As a consequence, the active species can diffuse on the surface in all the directions around the anatase microdomains. The surface diffusion coefficient of the active species on amorphous titania being isotropic, the isoconcentration lines of the diffusing species around the microdomain should almost be circular. This contrasts with the anisotropic evolution of the pits edges strongly suggesting, at first glance, that the photodegradation kinetics is governed by the reaction at the edges which is related the anisotropic properties of the SA crystal. This is also clearly evidenced by the linear evolutions of the gap distances as a function of irradiation time observed in Fig. 4 [20]. In the following, we try to correlate the morphology of the pits with the crystal properties.

By searching through the literature, we were astonished by the remarkable similarity between the observed morphology of the pits and the crystal habits of stearic acid as predicted by morphological simulations based on the attachment energy theory [15,21]. The latter, initially proposed by Hartman and Perdock [22], takes into account the intermolecular interactions (Van der Walls, hydrogen bonds) within the crystal to predict the crystal habit. The concept of attachment energy has been defined by these authors as the energy released per unit cell content per mole $E_{att}(hkl)$ upon the attachment of a crystal slice of thickness d_{hkl} on a face (hkl). Hartmann and Perdock demonstrated that the growth rates of a given (hkl) face is proportional to the absolute value of the attachment energy. The growth rate governs the crystal habit in that the faces showing the slowest growth rates will be the most morphologically

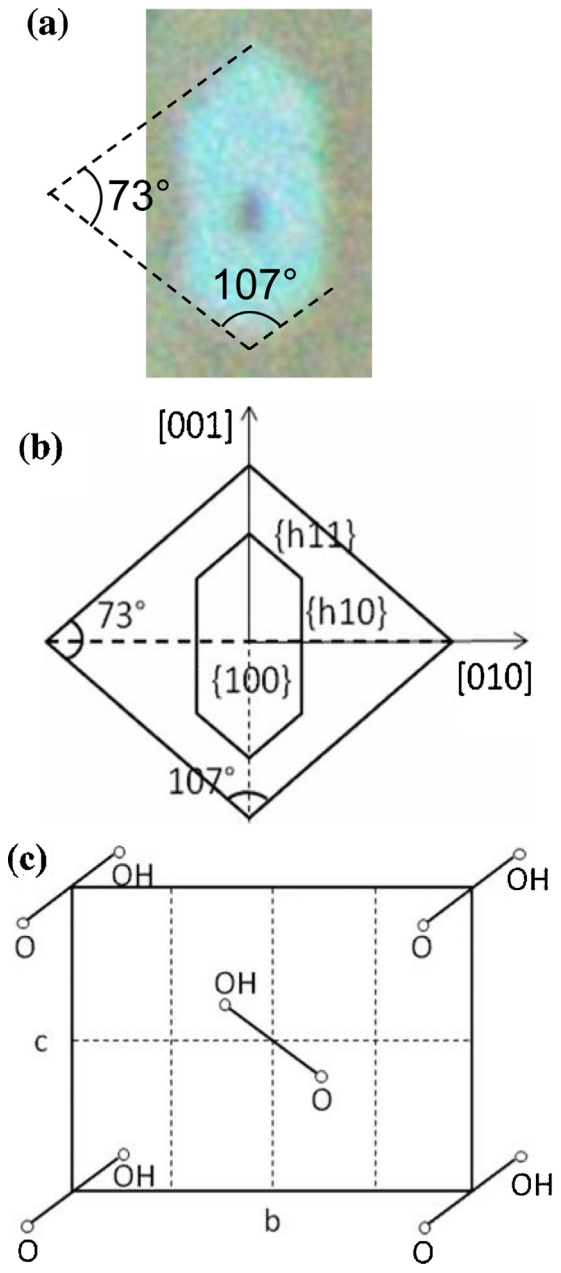

Fig. 4. (a) RL-DIC microscopy image of a representative dip within the stearic acid crystal (B-polymorph) after several minute ultraviolet irradiation (b) respective morphologies and orientations of the SA crystal and the pit edges in the bc plane of the unit cell (c) Projection of the unit-cell basal plane (bc plane) of the monoclinic B-form of stearic acid (adapted from Refs. [13,15]).

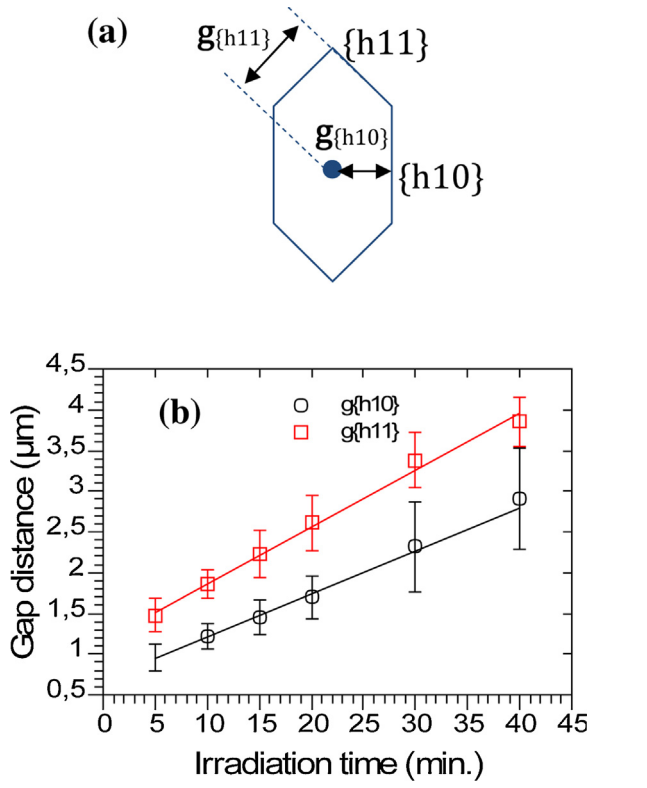

Fig. 5. (a) Definition of the gap distances $g_{\{h11\}}$ and $g_{\{h10\}}$ between the active microdomain the edges of the pits according to the {h11} and {h10} faces, respectively and (b) their evolution as a function of ultraviolet exposure time. The solid lines correspond to a linear fit.

pronounced. Further details concerning the Hartman and Perdok model and the evaluation of the attachment energy can be found in Refs. [15,21,22]. As a conclusion, the observed similarity between the calculated crystal habits of SA and the observed morphology of the pits (Figs. 2 and 3) are certainly not fortuitous but share the common feature of the interactions between the molecules within the crystal.

Table 2 lists the calculated attachment energies and interplanar spacing of the low index faces of the monoclic form of the B-polymorph of stearic acid obtained from Ref. [15]. The relative values of attachment energy can be rationalized in term of molecular arrangement within the crystal due to the relative orientation of the methyl and carboxyl groups. As an illustration, Table 2 shows that the {1 0 0} faces have an attachment energy which absolute value is much lower than both other faces sets. This can be explained by the fact that {1 0 0} faces are terminated with methyl groups conducting to methyl–methyl interactions [15]. These latter are very weak compared to the stronger lateral molecular interactions inside the bilayer which are mainly attributed to hydrogen bonds. The considerable correlation between the velocity of the edges (obtained from Fig. 5) and the relative attachment energy of the {1 1 0} and the {2 1 1} faces (Table 2) suggests that the attachment energy is also, somehow, the controlling factor of the morphology of the pits. In fact, the relative values of the attachment energy implicitly reflect the anisotropy of the bond strength within the crystal and thus the chemical groups terminating the different faces. Since the photodegradation of the SA proceeds via the formation and diffusion of active species such as $OH^{\bullet}$ or H_2O_2, one can suggest that the relative velocity of the pit edges is related to the relative chemical affinity of the active species for the chemical groups terminating a given crystal face.

Carboxylic acids are known to form strong hydrogen bonds with H-atom donors such as hydroxyl radicals and peroxide molecules [23]. The forces between OH and the co-reagent can affect the reaction dynamics and hence its kinetics. We could propose that the energy barrier seen by the active species reaching the pit edges might be then correlated to the anisotropy of the bond strength within the crystal. It should be significantly lowered for crystal faces showing high absolute value of attachment energy explaining the differences between the progression rates of the edges. This corresponds to the faces presenting favorably oriented co-reagents and for which the reaction is likely to involve hydrogen bonds.

Table 2
Calculated attachment energies (from Ref. [15]) and interplanar spacing of the low index faces of the B_m polytype of stearic acid. Displacement rate R_{hkl} of the pit edges according to the {hkl} faces.

{hkl}	Multiplicity	d_{hkl} (Å)	Attachment energy (kJ/mol)	R_{hkl} ($\mu m\,min^{-1}$)
{100}	2	43.95	−7.2	–
{110}	4	7.29	−83	0.057
{211}	4	4.38	−104.9	0.069

5. Conclusion

We have shown that the direct observation of the TiO_2 photocatalytic surface reaction, using RL-DIC microscopy, provides new insights into the reaction kinetics and degradation mechanisms of SA on TiO_2. The degradation of the SA crystals (B-polymorphs here) was observed to be initiated at the titania domains and form pits whose edges proceed along specific crystallographic directions of the SA crystal and with different velocities. First, these results provide further evidence that molecules well-separated from a photoactive titania domain can be photodegraded via the diffusion of active species. We proposed that the main factor governing the growth of a molecular crystal, the attachment energy, can also be invoked to explain the orientation and morphology of the pits. This analogy makes sense since the relative values of the attachment energy implicitly reflect the chemical groups terminating the different faces. Thus, the interactions between the diffusing active species and the SA molecules should be dependent on the crystalline orientation with consequences on the reaction dynamics and kinetics.

Acknowledgements

This work has been supported by the Erasmus Mundus Program E-GOV-TN (European Union—Project n° 2013-2434). The authors are grateful to Jean-Luc Pierrot for the AFM measurements and to Pascal Franchetti for the micro-raman measurements.

References

[1] Y. Paz, A. Heller, J. Mater. Res. 12 (1997) 2759–2766.
[2] A. Mills, A. Lepre, N. Elliott, S. Bhopal, I.P. Parkin, S.A. O'Neill, J. Photochem. Photobiol. A 160 (2003) 213–224.
[3] A. Mills, J. Wang, J. Photochem. Photobiol. A 182 (2006) 181–186.
[4] V. Romeas, P. Pichat, C. Guillard, T. Chopin, C. Lehaut, New J. Chem. 23 (1999) 365–373.
[5] P. Sawunyama, L. Jiang, A. Fujishima, K. Hashimoto, J. Chem. Phys. B 101 (1997) 11000–11003.
[6] P. Sawunyama, A. Fujishima, K. Hashimoto, Langmuir 15 (1999) 3551–3556.
[7] T. Remillard, J.R. MacBride, K.E. Nietering, A.R. Drews, X. Zhang, J. Phys. Chem. B 104 (2000) 4440–4447.
[8] M.N. Ghazzal, N. Barthen, N. Chaoui, Appl. Catal. B: Environ. 103 (2011) 85–90.
[9] M. Bahtat, C. Bovier, J. Serughetti, Mater. Chem. Phys. 32 (1992) 203–206.
[10] I.A. Alhomoudi, G. Newaz, Thin Solid Films 517 (2009) 4372–4378.
[11] G.J. Exarhos, M. Aloi, Thin Solid Films 193/194 (1990) 42–50.
[12] E. von Sydow, Acta Cryst. 8 (1955) 557.
[13] V. Malta, G. Celotti, R. Zanetti, A. Ferrero Martelli, J. Chem. Soc. B 54 (1971) 548–553.
[14] K. Sato, M. Kobayashi, H. Morishita, J. Cryst. Growth 87 (1988) 236–242.
[15] E. Moreno-Calvo, T. Calvet, M.A. Cuevas-Diarte, D. Aquilano, Cryst. Growth Des. 10 (2010) 4262–4271.
[16] D.B. Murphy, Fondamentals of Light Microscopy and Electronic Imaging, Wiley-Liss, United States, 2001.
[17] T. Tatsuma, S. Tachibana, A. Fujishima, J. Phys. Chem. B 103 (1999) 8033–8035.
[18] H. Haick, Y. Paz, J. Phys. Chem. B 105 (2001) 3045–3051.
[19] M.C. Lee, W. Choi, J. Phys. Chem. B 106 (2002) 11818–11822.
[20] D. Ollis, Appl. Catal. B: Environ. 99 (2010) 478–484.
[21] J. Evans, A.Y. Lee, A. Myerson, Crystallization and Solidification Properties of Lipids, in: N. Widlak, R.W. Hartel, S. Narine (Eds.), AOCS, Press, United States, 2001, pp. 17–33.
[22] P. Hartman, W.G. Perdok, Acta Crystallogr. 8 (1955) 49–57.
[23] I.W.M. Smith, A.R. Ravishankara, J. Phys. Chem. A 106 (2002) 4798–4807.